Proceedings of the
International Conference on Mechanical Engineering 2011
(ICME2011) 18-20 December 2011, Dhaka, Bangladesh

ICME11-IL-001

MICROFLUIDIC BASED LAMINAR FLOW FUEL CELL FOR PORTABLE POWER

Prashanta Dutta and Isaac B. Sprague

Microscale Thermo Fluid Laboratory, School of Mechanical and Materials Engineering
Washington State University, Pullman, Washington 99164-2920, USA
Email: prashanta@wsu.edu

ABSTRACT

2D numerical model is developed for a laminar flow fuel cell considering ion transport and the electric double layer (EDL) around the electrodes. The Frumkin-Butler-Volmer equation is used for the fuel cell kinetics. The finite volume method is used to form algebraic equations from governing partial differential equations. The numerical solution was obtained using Newton's method and a block tridiagonal matrix algorithm (TDMA) solver. The model accounts for the coupling of charged ion transport with the electric field and is able to fully resolve the diffuse regions of the electric double layer in both the stream-wise and cross-channel directions. Numerical results show that the concentration distributions for both the neutral species and ions change in the cross-stream direction as well as in the stream-wise direction. An especially interesting result is the change in positive ion concentration within the electrical double layer along the stream-wise direction. This model allows us to study both kinetically active (electrodes) and inactive (insulated wall) regions for a microfluidic fuel cell. This mathematical model and numerical simulation will be particularly useful in analyzing the complex behavior that occurs in laminar flow electrochemical devices where a minimum of two spatial dimensions must be considered and the electrical double layer and ion transport cannot be neglected.

Keywords: Microfluidics, Laminar Flow Fuel Cell, Electrode Kinetic, Electric Double Layer.

1. INTRODUCTION

In the past decade, the paradigm of using micro fuel cells for portable power applications has inspired novel innovations in fuel cell technology. One such example is the laminar flow fuel cell (LFFC) which utilizes colaminar flow to maintain the separation between the anode and cathode instead of a solid electrolyte such as the membrane used in polymer electrolyte membrane (PEM) fuel cells. The original concept of a LFFC was first presented as a vanadium redox cell in 2002 [1]. LFFCs were then investigated experimentally by addressing parameters such as flow rates and fuel concentrations [2-4]. Further adaptations of the original LFFC concept have also been proposed, usually focusing on the electrode structure such as an air breathing cathode [5-6], electrodes comprised of graphite rods aligned in the streamwise direction [7], and reactants fed through porous electrodes [8], among others.

In literature, there exist a number of models for laminar flow fuel cells [9-11]. These models assume that the electrolyte is electrically neutral throughout the channel and produce a linear electric potential gradient across the channel. Hence, these models simplify ionic transport in the electrolyte by using a charge conservation equation to model the electric potential. These simplified models have two obvious limitations. First, the transport equations do not explicitly consider the electromigration effects of charged ions, which is the main driving mechanism for the ion transport from the anode to the cathode. Second, these models neglect the electric double layer effects at the electrode-electrolyte interface that have been shown to play an important role in electrochemical kinetics [12]. In order to capture these complex electrochemical phenomena, a more fundamental model is necessary.

In this study a more general set of continuum equations that do not assume electroneutrality and include ion transport in the electrolyte are considered. This model accounts for the strong coupling between charged ions and the electric potential, and has been used to model the ionic migration and the diffuse double layer in electrochemical cells [13-15]. The model is also able to capture the electric double layer and flow effects in electrochemical kinetics. The electric double layer plays a major role in the overall cell potential and the charge transfer kinetics at the electrode-electrolyte interface.

This allows for the more accurate Frumkin-Butler-Volmer equation for kinetics by using the local concentration of reactants at the Stern layer-diffuse layer interface and the potential drop across the Stern layer.

2. THEORY

In a laminar flow fuel cell (Fig. 1), fuel (F) is oxidized at the anode which frees cations (C) and electrons (e^-) that are then consumed at the cathode along with the oxidant (O) to produce current. Therefore, the stoichiometric equations for the half reactions at the electrodes become:

$$Anode: s_F \cdot F \rightarrow s_C \cdot C + n \cdot e^- \quad 1(a)$$

$$Cathode: s_C \cdot C + n \cdot e^- + s_O \cdot O \rightarrow waste \quad 1(b)$$

and the overall redox reaction becomes

$$Overall: s_F \cdot F + s_O \cdot O \rightarrow Waste \quad 1(c)$$

The parameter n represents the number of electrons released by fuel oxidation and consumed by oxidant reduction. Its value depends on the type of fuel used in the overall reaction, i.e., for hydrogen $n = 2$ and for methanol $n = 6$. The stoichiometric coefficient, s, is the number of molecules of a given species that react with n electrons. The rate at which the half reactions proceed is governed by the Frumkin-Butler-Volmer equation for anode and cathode as:

$$j = Fn\vec{k}_{An} c_F e^{(1-\beta)\Delta\phi_S zF/RT} - Fn\vec{k}_{An} c_C e^{-\beta\Delta\phi_S zF/RT} \quad 2(a)$$

$$j = Fn\vec{k}_{Ca} e^{(1-\beta)\Delta\phi_S zF/RT} - Fn\vec{k}_{Ca} c_O c_C e^{-\beta\Delta\phi_S zF/RT} \quad 2(b)$$

where the concentration terms for the reactants are obtained from the continuum distribution of the concentration fields c_F, c_O, c_C, taken at the electrode of interest. It should be noted that the electric double layer will have significant impact on the value of c_C at the electrode.

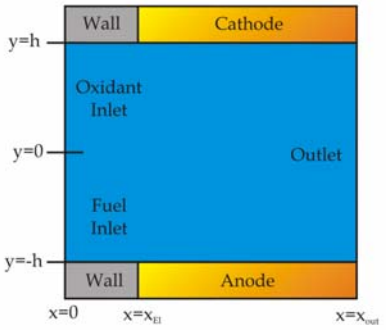

Fig 1. The computational domain considered for the model depicting a main channel with two inlet streams. Anode and cathode reaction regions starts at $x=x_{El}$.

2.1 Mathematical Model

The flux density of the reactant species and the electrolyte components is given by

$$N_i = \vec{v}c_i - D_i \nabla c_i - z_i \omega_i F c_i \nabla\phi \quad (3)$$

where i indicates the specific species and $i = C, A, F, O$. The flux density is comprised of three components: advection, diffusion, and electromigration. The first term on the right hand side of equation (3) is advection; this term is important to consider for LFFCs which have a flowing liquid electrolyte. The second term is diffusion and the third term is electromigration, which is critical to the function of fuel cells because it is the primary motive force for the charged ions to migrate from one electrode to the other. It is obvious from equation (3) that the flux density of a charged ion is dependent on the electrolyte potential gradient.

The concentration distributions are governed by the steady state Nernst-Plank equation which reduces to

$$\nabla \cdot N_i = 0 \quad (4)$$

The potential distribution in the electrolyte is governed by Poisson's equation

$$-\nabla \cdot (\varepsilon_E \nabla\phi) = F \sum z_i c_i \quad (5)$$

Here, the right hand side of the equation is the charge density, which is the sum of the total charge for all of the species present. For neutral species such as fuel and oxidant, the ionic charge is zero so they do not contribute to the total charge density.

The flow field is governed by the steady state Navier-Stokes and continuity equations as [11]:

$$\nabla \cdot (\rho\vec{v}\vec{v}) = \nabla \cdot (\mu\nabla\vec{v}) - \nabla p \quad (6a)$$

$$\nabla \cdot (\rho\vec{v}) = 0 \quad (6b)$$

2.2 Boundary Conditions

For a 2D planar microchannel, there exist six different kinds of boundaries: fuel inlet, oxidant inlet, wall, anode electrode, cathode electrode, and outlet. Hence, six sets of boundary conditions are required for each unknown variable. The inlet streams provide a specified concentration for each species. The fuel inlet specifies the fuel concentration and has no oxidant influx and vice versa for the oxidant inlet. It is assumed that at the inlet the potential has an insulation condition. Therefore the boundary conditions for the electrochemical governing equations at the fuel inlet are:

$$c_C = c_A = c_E \quad (7a)$$

$$c_F = c_{F,in} \quad (7b)$$

$$c_O = 0 \quad (7c)$$

$$\frac{\partial\phi}{\partial x} = 0 \quad (7d)$$

and at the oxidant inlet are:

$$c_C = c_A = c_E \quad (8a)$$

$$c_O = c_{O,in} \quad (8b)$$

$$c_F = 0 \quad (8c)$$

$$\frac{\partial \Phi}{\partial x} = 0 \quad (8d)$$

At the outlet it is assumed that the transport phenomenon is fully developed and therefore is no longer functions of the x direction. This translates to the assumption that there are no concentration gradients along the channel axis and there is no change in electrolyte potential:

$$\frac{\partial c_C}{\partial x} = \frac{\partial c_A}{\partial x} = \frac{\partial c_F}{\partial x} = \frac{\partial c_O}{\partial x} = 0 \quad (9a)$$

$$\frac{\partial \Phi}{\partial x} = 0 \quad (9b)$$

The channel wall, in the absence of an electrode, provides a zero flux condition for the mass transport equations. It is also assumed that the wall is an insulator and has no surface charge yielding a zero potential gradient normal to the surface. As a result the boundary conditions at the wall are:

$$D_C \frac{\partial c_C}{\partial y} - z_C \omega_C F c_C \frac{\partial \Phi}{\partial y} = 0 \quad (10a)$$

$$D_A \frac{\partial c_A}{\partial y} - z_A \omega_A F c_A \frac{\partial \Phi}{\partial y} = 0 \quad (10b)$$

$$D_F \frac{\partial c_F}{\partial y} = 0 \quad (10c)$$

$$D_O \frac{\partial c_O}{\partial y} = 0 \quad (10d)$$

$$\frac{\partial \Phi}{\partial y} = 0 \quad (10e)$$

The electrodes are the most important part of a fuel cell where interesting electrochemical interactions occur, and are of paramount importance for fuel cell operation. At the electrodes, the non-reacting species have a zero flux condition, while the reacting species have a flux equal to the ionic current density which is related to the electric current density by the Faraday constant, number of cations involved in the reaction and a stoichiometric coefficient derived from the reaction equations (Eq. 1). The sign of the flux is determined by the species position in the stoichiometric equation, i.e., negative if the species is a reactant and positive if the species is a product. Therefore, for the mass transport equations, the anode boundary conditions are:

$$D_C \frac{\partial c_C}{\partial y} - z_C \omega_C F c_C \frac{\partial \Phi}{\partial y} = \frac{s_C j}{nF} \quad (11a)$$

$$D_A \frac{\partial c_A}{\partial y} - z_A \omega_A F c_A \frac{\partial \Phi}{\partial y} = 0 \quad (11b)$$

$$D_F \frac{\partial c_F}{\partial y} = -\frac{s_F j}{nF} \quad (11c)$$

$$D_O \frac{\partial c_O}{\partial y} = 0 \quad (11d)$$

For the electrolyte potential at the boundary, an adaptation of the Stern model for the inner layer is used [16]. Here, the boundary value is determined by the electrode potential plus the drop across the Stern layer, $\phi = \psi + \Delta\phi_S$, where the potential is assumed to be linear and continuous with the potential in the electrolyte. The Stern layer thickness is determined by the ratio of the permittivity in the Stern layer over the capacitance of the Stern layer. For the anode electrode, the boundary condition for electrolyte potential is:

$$\Phi = \Psi_A + \frac{s_3}{C_s} \frac{\partial \Phi}{\partial y} \quad (11e)$$

Similarly the boundary conditions for cathode (electrode) are:

$$D_C \frac{\partial c_C}{\partial y} - z_C \omega_C F c_C \frac{\partial \Phi}{\partial y} = -\frac{s_C j}{nF} \quad (12a)$$

$$D_A \frac{\partial c_A}{\partial y} - z_A \omega_A F c_A \frac{\partial \Phi}{\partial y} = 0 \quad (12b)$$

$$D_F \frac{\partial c_F}{\partial y} = 0 \quad (12c)$$

$$D_O \frac{\partial c_O}{\partial y} = -\frac{s_O j}{nF} \quad (12d)$$

$$\Phi = \Psi_C + \frac{s_3}{C_s} \frac{\partial \Phi}{\partial y} \quad (12e)$$

It should be noted that the drop across the Stern layer will be negative for the anode and positive for the cathode except in the case of very low cell potentials.

The boundary conditions for momentum and mass conservation equations are straightforward. We assumed a fully developed velocity distribution in both fuel and oxidant inlet channels and therefore prescribed the fluid velocity profile as parabolic flow at each inlet. There exists a no slip and no penetration boundary conditions at the wall and electrodes. Finally, the pressure is specified as zero gauge at the outlet.

$$Inlet: \ \vec{v} = \vec{v}_{in} = v_{Max}\left[1 - \left(\frac{2(|y| - L/2)}{L}\right)^2\right] \cdot \vec{i} \quad (13a)$$

$$Outlet: \ p = 0 \quad (13b)$$

$$Walls: \ \vec{v} = 0 \quad (13c)$$

3. NUMERICAL FORMULATION

The governing equations used to describe the laminar flow fuel cell are nonlinearly coupled, and hence for a two dimensional domain the system of equations must be solved numerically. In this study the finite volume method is used to form algebraic equations. The finite volume method breaks the domain down into discrete volumes. This allows the fluxes across the finite volumes to be calculated at each control point. One of the major advantages of the finite volume method is the conservation of the flux across the domain [17-20].

Since the fluid flow equations (Eq. 6) are not influenced by the parameters solved in equations (4 and 5), they can be solved separately from, and prior to equations 4 and 5. The system of equations used for fluid flow is nonlinear and suffers from the lack of a pressure equation. Fortunately, there has been significant work on solving these equations using the finite volume technique. For this work, the co-located Semi-Implicit Method for Pressure-Linked Equations (SIMPLE) algorithm is used [14].

The system of equations used to describe electrochemical system (Eqs. 4 & 5) is also nonlinear and highly coupled. This yields a set of nonlinear algebraic equations that are not straightforward to solve, and

cannot be solved with tridiagonal matrix algorithm (TDMA) or Gauss-Seidel methods often used in conjunction with the finite volume method. Here, Newton's method is applied for a system of equations, which offers two distinct advantages [14]. First, all the transport equations and the Poisson's equation can be solved simultaneously, a necessity due to their strongly coupled nature. Second, the Newton's method converts the nonlinear system of algebraic equations to a linear set.

For this study, a parallel algorithm is developed to solve both flow and electrochemical equations concurrently. By implementing a parallel solver, significant computational time savings can be obtained. In this work, an Intel Core i7-975 3.33GHz processor with 4 cores was used. The numerical results were completed in 4.72 hours using 4 threads, while it took 12.5 hours for a single thread.

4. RESULTS AND DISCUSSION

4.1 Fuel and Oxidant Distribution

A laminar flow fuel cell operating under partial load, away from open or short circuit, with flowing electrolyte is considered. For the numerical results, the electrode potentials are set as $\psi_{Ca} = -\psi_{An} = 76$ mV, the kinetic rate constants are $\vec{k}_{An} = 4.658\times10^{-5}\, m/s$ and $\vec{k}_{An} = 4.658\times10^{-7}\, m/s$ for the anode and $\vec{k}_{Ca} = 8.782\times10^{-9}\, mol/m^2\cdot s$ and $\vec{k}_{Ca} = 9.883\times10^{-8}\, m^4/mol\cdot s$ for the cathode. The stoichiometric coefficients are $s_F = 1, s_O = 1, s_C = 6$ and the number of electrons involved in the kinetic reaction (n) is 6. The inlet velocity profile for each inlet is set to the steady state flow profile for a rectangular duct.

The concentration profiles for the full domain are shown as contour plots in figures 2(a) and 2(b) for fuel and oxidant, respectively. The formation of a depletion boundary layer can be seen near the anode $(y \to -h)$ in figure 2a and close to the cathode $(y \to h)$ in figure 2b. The boundary layer starts at the upstream side of the electrode. As the fuel and oxidant are consumed by the electrode kinetics, they are depleted from the fluid. The further downstream of the cell, the more reactants have been consumed. If the current is large enough that all the reactants at the electrode are consumed and cannot be replenished by diffusion from the bulk flow, the kinetics for that electrode will become transport limited. These figures also show that fuel and oxidant remain mostly unmixed in the channel. At the channel inlet (in figure 2a), the fuel is specified to the inlet concentration for the entire fuel inlet, and not present at the oxidant inlet.

The contour plots show the results for the entire domain for (a) fuel and (b) oxidant. The diffusion coefficient for the neutral species is ten times less than the diffusion coefficient of the cations. The Stern layer capacitance is $C_S = 80\,\mu F/cm^2$ and the Stern layer permittivity is ten times that of the permittivity in a vacuum, $\varepsilon_S = 10\cdot\varepsilon_{vaccum}$. Here $c_0 = 94.26\ mM$.

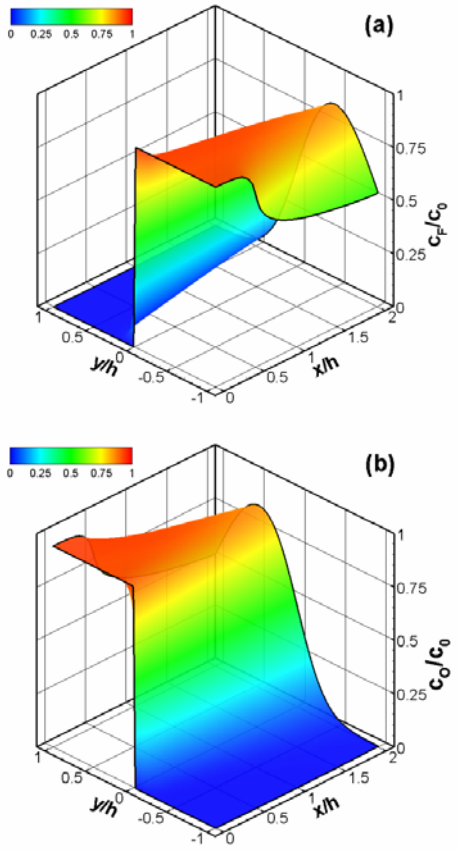

Fig 2. Concentration distributions for the neutral species.

As the flow progresses downstream, the fuel begins to diffuse into the oxidant side. This is known as transverse diffusional mixing. If the concentration of fuel at the cathode increases above zero it can oxidize there, effectively short circuiting the fuel cell. This is known as fuel crossover and it can be very detrimental to fuel cell performance. In a laminar flow fuel cell, there is no physical separation between the anode and the cathode; fuel crossover is prevented by controlling the operating parameters such that the separation of neutral species is maintained. This behavior cannot be captured by previous electrochemical models that included electric double layer, but did not consider the flow effects [16].

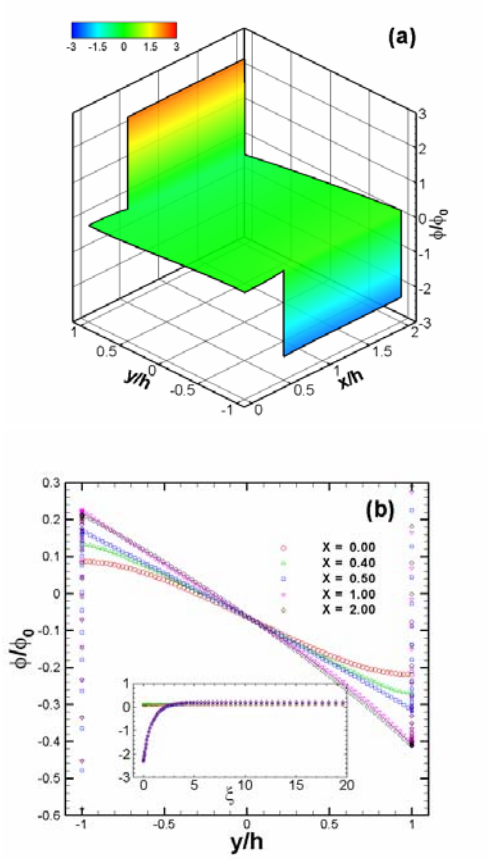

Fig 3. Distribution of potential in the electrolyte for the case of $\phi_{An} = -3\phi_0, \phi_{Ca} = 3\phi_0$ & $\phi_0 = 25.7$ mV . The (a) contour plots show the results for the entire domain and (b) specific cross channel results for different locations along the channel. The inset in (b) shows the near wall potential distribution against the inner scale (ξ).

4.2 Potential Distribution

The potential distribution in the electrolyte for the full domain is shown in figure 3a. The electric double layer shape matches expected results in the cross channel direction. The results presented in figure 3b are the same as those presented in the contour plot but show the behavior of the potential across the channel for different positions along the channel. The potential drop across the channel, especially in the bulk fluid (away from the electrodes), can clearly be seen. Further downstream, the potential drop becomes more linear. However, according to the 1D analytical solution, it will never become linear when current across the cell is present [16]. This potential drop is known as the cell's internal resistance in the fuel cell community. The potential distribution across the channel at the inlet is not flat as shown in figure 3a and 3b. This is due to the fact that the upstream potential is influenced by the potential distribution between the electrodes. If the distance between the inlet and the start of the electrodes was large enough, then the potential distribution at the inlet would be flat.

The inset in figure 3b shows the potential distribution near the (anode) electrode. The evolution of the electric double layer at the electrode is very quick and the potential distribution reaches a stable shape just downstream of the start of the electrode; so if the channel length were increased the shape of the electric double layer wouldn't change. Also the lack of a double layer at the insulated wall $(x = 0, x = 0.4h)$ can be seen in the inset of figure 3b. The developing behavior of the electric double layer along a channel cannot be captured by 1D results.

4.3 Ion Distribution

The concentration distributions of the ions are presented in figure 4. Figure 4a shows the concentration distribution of the cation. The positively charged cations are attracted towards the anode electrode which is negatively charged. As the fuel oxidizes in the anodic side, positively charged cations are released into the electrolyte and negatively charged electrons are transferred into the electrode. These electrons build up causing a net negative charge in the anode. The opposite phenomenon occurs in the cathodic side, where electrons are consumed from the electrode and combined with cations in the electrolyte. The electron depletion from the cathode electrode results in a net positive charge in the cathode electrode. This positive charge repels the cations resulting in depletion of cations in the electrolyte at the cathodic side. Similarly but opposite for the anion, shown in figure 4b, where there is a depletion of anions at the anode and a buildup of anions at the cathode in the electrolyte.

Consider the anodic side in figures 4a and 4b; the local increase in cation concentration is greater than the local decrease in anion, which is consistent with EDL theory. The net charge in the EDL must be equal and opposite to the net charge in the solid electrode. However, the anion concentration can only decrease to zero near the electrode so the remaining difference must be accounted for by a larger excess of cations.

It can be seen that the shape of the anion and cation distribution follows closely the shape of the potential distribution. This is a direct result of the strong coupling between the potential and ion distributions. *This distribution of ions throughout the domain cannot be properly captured by models that neglect the coupling between potential and ion transport.* A very interesting observation is apparent in figure 4a where the concentration of cations near the anode increases as the fluid progresses downstream. Similarly the concentration of anions at the cathode in figure 4b decreases.

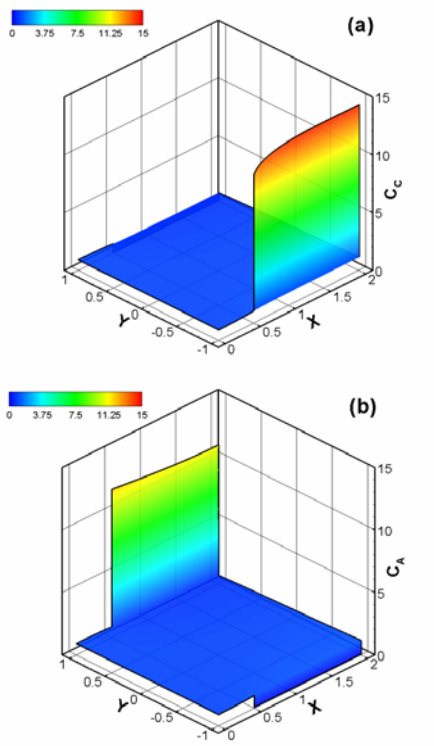

Fig 4. Normalized concentration distributions for the ions. The contour plots show the results for the entire domain for (a) cation and (b) anion.

4.4 Cell Performance

Two important parameters to evaluate fuel cell performance are cell potential and current density. The cell potential can be calculated as $\Psi_{Cell} = \Psi_{Ca} - \Psi_{An}$ using the input electrode potentials, and the cell current density can be calculated by integrating the current density along one of the electrodes:

$$I_{An} = \frac{1}{(X_{out} - X_{El})} \int_{X_{El}}^{X_{out}} j_{An}(X)\, dX \qquad (14)$$

A positive cell current correlates a positive anode current and a negative cathode current by convention. If the governing equations and accompanying boundary conditions are solved for different values of Ψ_{Cell} (Ψ_{An}, Ψ_{Ca}) ranging from zero (short circuit) up until $I_{Cell} = 0$ (open circuit) then a classic fuel cell analysis plot, the Voltage-Current plot, can be created.

Figure 5 shows a V-I plot for a fuel cell operating at the same kinetic and flow parameters considered above. The anode electrode potential $\Delta\Psi_A = (\Psi_A - \Phi_{Y=0})$ and cathode electrode potential $\Delta\Psi_C = (\Psi_C - \Phi_{Y=0})$, are also shown in Figure 5. For the anode, the more negative the electrode potential, the lower the current density. The opposite is the true for the cathode, i.e., the more positive the electrode potential the lower the current density. Figure 5 shows that the cell is anode limited when operating as a short circuit. i.e., the anode electrode potential is less negative than the cathode electrode potential is positive. However at open circuit, the cathode electrode potential is greater than the anode electrode potential and the cell is cathode limited.

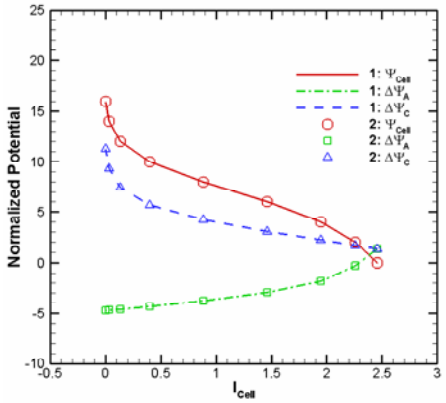

Fig 5. Voltage-Current plots for the laminar flow fuel cell. Shown is the total cell voltage, $\Psi_{Cell} = \Psi_{Ca} - \Psi_{An}$, the anode electrode potential $\Delta\Psi_A = (\Psi_A - \Phi_{Y=0})$, and the cathode electrode potential $\Delta\Psi_C = (\Psi_C - \Phi_{Y=0})$.

5. CONCLUSIONS

A 2D numerical model is developed for a laminar flow fuel cell considering ion transport and EDL around the electrodes. Finite volume method is used to form algebraic equations from governing partial differential equations. The numerical solution was obtained using Newton's method for a system of equations and a block TDMA solver. Different operating phenomena such as the laminar flow separation, the development of the depletion boundary layers and EDL, and the coupling of ion transport with electric potential were shown. The model was also able to show the shape of the EDL in the downstream direction as well as how the double layer changes along the electrode. These numerical results demonstrate the model's ability to capture the complex behavior of such a device.

ACKNOWLEDGMENT

This research was partly supported by the 2010 KU Brain Pool Program of Konkuk University, Korea, and by the School of Mechanical and Materials Engineering of Washington State University.

6. REFERENCES

1. Ferrigno, R., Stroock, A. D., Clark, T. D., Mayer, M., Whitesides, G. M., "Membraneless Vanadium Redox Fuel Cell Using Laminar Flow" *J. American Chemical Society 2002,* **124** 12930-12931.
2. Choban, E. R., Markoski, L. J., Wieckowski, A., Kenis, P. J. A., "Microfluidic Fuel Cell Based on Laminar Flow"*J. Power Sources 2004,* **128** 54-60.
3. Sprague, I., Dutta, P., and Ha, S., "Flow Rate Effect on Methanol Electro-oxidation in a Microfluidic Laminar Flow System"*J. New Materials for Electrochemical Systems 2010*.
4. Sprague, I. B., Dutta, P., Ha, S., "Characterization of

a Membraneless Direct-Methanol Micro Fuel Cell" Proc. *IMechE Part A: J. Power and Energy 2009,* **223** 799-808.
5. Jayashree, R. S., Gancs, L., Choban, E. R., Primak A., Natarajan, D., Markoski, L. J., Kenis, P. J. A., "Air-Breathing Laminar Flow-Based Microfluidic Fuel Cell"*J. American Chemical Society 2005,* **127** 16758-16759.
6. Jayashree, R. S., Egas, D., Spendelow, J. S., Natarajan, D., Markoski, L. J., Kenis, P. J. A., "Air-Breathing Laminar Flow-Based Direct Methanol Fuel Cell with Alkaline Electrolyte" *Electrochemical and Solid-State Letters 2006,* **9** A252-A256.
7. Kjeang, E., McKechnie, J., Sinton, D., Djilali, N., "Planar and Three-deimensional Microfluidic Fuel Cell Architectrues Based on Graphite Rod Electrodes" *J. Power Sources 2007,* **168** 379-390.
8. Kjeang, E. Michel, R., Harrington, D. A., Djilali, N. Sinton, D., "A Microfluidic Fuel Cell with Flow-Through Porous Electrodes" *J. American Chemical Society 2008,* **130** 4000-4006.
9. M.-H. Chang, F. Chen, and N.-S. Fang, Analysis of Membraneless Fuel Cell Using Laminar Flow in a Y-shaped Microchannel, J. of Power Sources, **159**, pp. 810-816, 2006.
10. F. Chen, M.-H. Chang, and C.-W, Hsu, Analysis of Membraneless Microfuel Cell using Decomposition of Hydrogen Peroxide in Y-shaped Microchannel, Electrochimica Acta, **52**, pp. 7270-7277, 2007.
11. F. Chen, M.-H. Chang, and M.-K. Lin, Analysis of Membraneless Formic Acid Microfuel Cell using a Planar Microchannel, Electrochimica Acta, **52**, pp. 2506-2514, 2007.
12. Bazant, M. Z., Chu, K. T., Bayly, B. J., "Current-Voltage Relations for Electrochemical Thin Films" *Siam J. Applied Mathematics 2005*, **65** 1463-1484.
13. Sprague, I.B., Byun, D., and Dutta, P., "Effects of Reactant Crossover and Electrode Dimensions on the Performance of a Microfluidic Based Laminar Flow Fuel Cell" *Electrochimica Acta 2010*, **55**, pp. 8579-8589.
14. Sprague, I.B. and Dutta, P., "Modeling of Diffuse Charge Effects in a Microfluidic Based Laminar Flow Fuel Cell" *Numerical Heat Transfer: Part-A, 2011*, **59**, pp. 1-27.
15. Sprague, I.B. and Dutta, P., "Role of Diffuse Layer in Acidic and Alkaline Fuel Cells" *Electrochimica Acta 2011*, **56**, pp. 4518-4525.
16. Bonnefont, A., Argoul, F., Bazant, M. Z., "Analysis of Diffuse-layer Effects on Time-dependent Interfacial Kinetics" *J. of Electroanalytical Chemistry 2001*, **500** 52-61.
17. Dutta, P., Beskok, A., Warburton, T. C., "Numerical Simulation of Mixed Electroosmotic/Pressure Driven microflows" *Numerical Heat Transfer: Part –A 2002*, **41**, pp. 131-148.
18. Patankar, S. V., Numerical Heat Transfer and Fluid Flow, 113-154, *Hemisphere Publishing Co. 1980*, USA.
19. Shim, J., Dutta, P., and Ivory, C. F. "Finite Volume Methods for Isotachophoretic Separation in Microchannel" *Numerical Heat Transfer: Part -A 2007*, **52** 441-461.
20. Shim, J., Dutta, P., and Ivory. C. F., "Parallel Implementation of Finite Volume Based Method for Isoelectric Focusing" *J. of Mechanical Science and Technology 2009*, **23** 3169-3178.

7. Nomenclature

Symbol	Meaning
C	capacitance
c	concentration
D	diffusion coefficien
e^-	electron
F	Faraday's constant
h	channel half heigh
I	total normalized current density
I	current density
J	normalized current density
$\vec{k}$	forward rate constan
$\overleftarrow{k}$	backward rate constant
N	flux density of species
p	pressure
R	universal gas constant
T	temperature
$\vec{v}$	velocity field
X	normalized position along the channel
x	position along the channel
Y	normalized position across the channel
y	position across the channel
z	ionic charge
Greek Letters	
β	kinetics symmetry factors
$\Delta\varphi_s$	potential drop across Stern layer
λ	Debye length
ξ	inner scale normalized by λ
ε	permittivity
μ	Viscosity
ρ	density
ϕ	electrolyte potential
Ψ	normalized electrode potential
ω	Mobility
Subscripts	
An	anode
C	cation
Ca	Cathode
Cell	cell
E	electrolyte
El	electrode
F	Fuel
in	inlet
O	Oxidant
out	outlet
S	Stern layer